6th International Conference on Advances in Experimental Structural Engineering
11th International Workshop on Advanced Smart Materials and Smart Structures Technology
August 1-2, 2015, University of Illinois, Urbana-Champaign, United States

Damage Identification in Unbonded Tendons for Post-tensioned Bridges

A.B.M. Abdullah[1], Jennifer A. Rice[2], H.R. Hamilton[3], Gary R. Consolazio[4]

1   PhD Candidate, Department of Civil and Coastal Engineering, University of Florida, Gainesville, FL 32611, USA.
    E-mail: abm.abdullah@ufl.edu
2   Assistant Professor, Department of Civil and Coastal Engineering, University of Florida, Gainesville, FL 32611, USA.
    E-mail: jrice@ce.ufl.edu
3   Professor, Department of Civil and Coastal Engineering, University of Florida, Gainesville, FL 32611, USA.
    E-mail: hrh@ce.ufl.edu
4   Associate Professor, Department of Civil and Coastal Engineering, University of Florida, Gainesville, FL 32611, USA.
    E-mail: grc@ce.ufl.edu

ABSTRACT

The use of flexible fillers in lieu of cement grout in post-tensioned bridges enables the application of new methods for detecting tendon damage. This paper presents two distinct monitoring approaches based on the anchor response and compares their effectiveness in wire breakage detection. The first method captures the static response of the strand to wire breaks through the change in strain distribution in anchors. The second method relies on the change in dynamic characteristics of the broken strand by detecting the shift in strand's natural frequencies after each wire break. The feasibility of these two methods have been separately investigated by analytical and experimental studies. To facilitate autonomous tendon monitoring, an efficient data processing algorithm has been developed with an optimized sensor arrangement. A sensitivity study has been carried out with random measurement errors to predict in-field performance of the proposed damage detection model. Extensive finite element analysis has been conducted with varying degrees of strand confinement to determine its effects on stress recovery and breakage detectability. The analysis provides useful insights into localized and global strand and anchor response that are pivotal for developing a robust tendon monitoring system. The numerical results have been subsequently verified by experimental findings.

KEYWORDS: *Tendon damage, Wire break detection, Unbonded tendon, Strand behavior, Finite elements.*

1. INTRODUCTION

Post-tensioning (PT) is widely used in bridge constructions because it offers numerous advantages over ordinary reinforced concrete, including more efficient use of materials, better deflection and crack control, durability, quicker construction, reduced cost, and design flexibility. The prestressing strands in PT structures, however, are prone to corrosion and require continuous surveillance for detecting wire failures. Although some of the existing tendon monitoring methods have been shown to perform well under favorable structural and ambient conditions, most of them are not found feasible in practice. In this paper, two approaches are presented in search of an efficient tendon monitoring system through an integrated experimental and analytical investigation.

A complete assembly of a PT system (tendon) typically comprises prestressing strands, anchorage, trumpets, ducts, deviators, and an anti-corrosion filler material (Fig. 1.1). The prestressing strand is a tensioning element, which is generally high-strength, low-relaxation steel made up of a group of helical outer wires and a straight center wire. The anchorage, consisting of a set of wedges, a wedge plate (or anchor head), and a bearing plate, is positioned at the ends of concrete girder for transferring tendon force into the concrete. The wedge (two- or three-part tapered steel pieces) grips the strand and seats on the wedge plate (usually an iron casting) that is placed against an iron bearing plate. The trumpet is an HDPE (high-density polyethylene) cone that connects the anchor to the duct and transitions the strands into a tight bundle to fit inside the duct. The plastic duct provides an opening in concrete (in an internally prestressed girder) that accommodates the prestressing steel and contains filler materials that occupy the voids between strands and duct. The deviator is a reinforced concrete casting (or steel fixtures embedded in the concrete) placed at specific locations to control the tendon profile in an externally prestressed girder.

Grout is commonly used in post-tensioned bridges as a filler material for protecting the tendon from corrosion. Once hardened, it bonds to the tensioned strands and to the inner wall of tendon duct, and thereby allows force transfer between the tendon and surrounding concrete. As a result, the bonded tendon provides structural redundancy to withstand accidental overload conditions. However, the tendon ducts are often not fully filled

with grout due to poor quality control during construction, which leaves the steel strands unprotected from corrosion. Consequently, several tendon failure events have occurred in the recent years in bonded post-tensioned bridges [1]. These failures have motivated the exploration of employing an unbonded system, in which a flexible filler, e.g., wax, is inserted into the tendon duct instead of cement grout. In the event of a wire break, the absence of grout in unbonded tendons allows the prestress loss to be transferred from the break to the end anchors, encouraging new tendon monitoring approaches based on global anchor response [2-4].
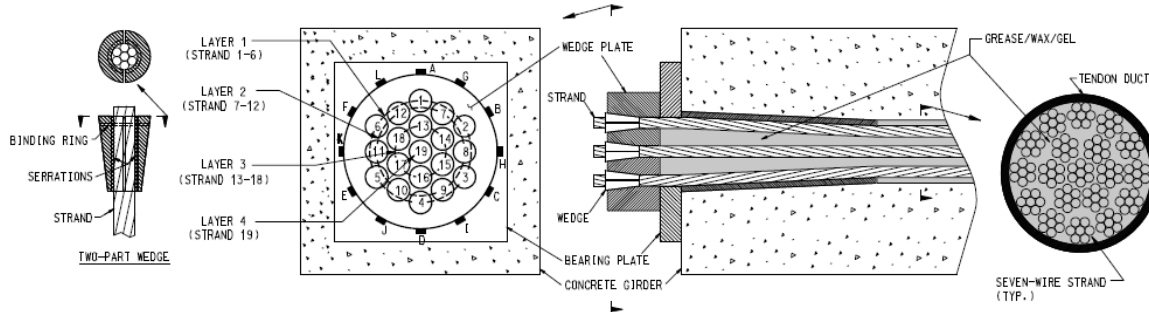

Figure 1.1 Unbonded PT system

While a dependable non-destructive monitoring method for unbonded tendons is not currently available, several attempts have been made recently for corrosion or defect detection and tendon force monitoring [5-12]. Some of these methods, such as visual inspection and screwdriver penetration test, are subjective and may not identify tension deficiencies or wire breakages away from inspection location. Imaging techniques (e.g., radiography) and magnetic methods (e.g., remnant magnetism (RM), magnetic flux leakage (MFL), magnetic permeability, and magnetostrictive sensing) are not suitable to operate on a daily basis. Vibration-based approaches that examine the change in modal properties of the entire bridge are insensitive to tendon defects. Active wave propagation methods (e.g., guided wave ultrasonic testing (GWUT), time-domain reflectometry (TDR), impact-echo (IE), and ultrasonic testing (UT) impulse-echo) and passive wave propagation methods (e.g., acoustic emission or AE), are susceptible to non-breakage events and therefore entails sophisticated filtering operations and data processing capabilities for removing possible false alarms. Electrically isolated tendons (EIT) and electro-mechanical impedance (EMI) measurement approaches require modifications in the existing construction practices. Other approaches, including georadar (ground penetrating radar or GPR), covermeter, various laser-based methods, potential mapping, thermography, and tomography have limited applicability in sensing tendon faults in their present form. These limitations of the existing methods, along with load transfer mechanism of unbonded tendons, have inspired the anchor-based monitoring approach presented in this paper.

2. SENSITIVITY OF STRAIN DISTRIBUTION IN ANCHORS TO WIRE BREAKS

Unlike bonded construction, unbonded tendons have limited contact points with the concrete girder, namely at the end anchors and deviators. Consequently, the entire prestress force is transferred to the girder only through these locations, which puts the wedge plates under heavy compressive strain. A wire break causes partial strain relief in the wedge plate and thus, alters its overall strain field. This change in strain distribution is a function of the severity of tendon damage (the number of wire breaks in a strand) and the location of the strand (or the wedge holding the broken strand) on the wedge plate (Fig. 1.1). The region of the wedge plate close to the broken strand experiences greater strain relief compared to a more distant region, resulting in differential strain distribution around the circumferential perimeter of the wedge plate. A thoughtful placement of strain sensors around the wedge plate can be useful in capturing this uneven strain change and to identify, locate, and quantify the tendon damage.

A set of experiments were performed to evaluate the levels of strain change on a 19-strand wedge plate with various wire break conditions by mechanically cutting the wires on different strand layers (grouping of strands based on their radial distance from wedge plate perimeter, shown in Fig.1.1). Due to capacity limitations of the stressing fixture, the experiments were conducted with a fully-populated but partially-stressed wedge plates (all the wedges were pre-seated but only a pair of strands were actively stressed during each test). To obtain a more realistic representation of strain variation with fully-stressed wedge plate, a finite element (FE) model of the anchorage assembly was created. The model was subsequently used to conduct a comprehensive parametric study with varying number and location of wire breaks.

2.1. Experimental evaluation of strain distribution in wedge plates

2.1.1. Test setup and procedure

Nineteen-strand wedge plates with a group of pre-seated wedges were placed at the ends of an approximately 1.5-m (5-ft) long stressing fixture (Fig. 2.1a). A hollow-core load cell was positioned at the dead end to monitor tendon force. The wedge plates were instrumented with 12 foil strain gauges (gauge length of 5 mm) to measure anchor strain in the direction parallel to strand's axis (Fig 2.1b, Fig. 1.1). The tested specimens were 15.2-mm (0.6-in) diameter, Grade 270, seven-wire prestressing strands [13] anchored to the wedge plates by two-part wedges. Three separate tests were carried out in which Strand 1, Strand 12, and Strand 13 were stressed to 74% of strand's capacity ($0.74F_u$) with a mono-strand jack in Test 1, Test 2, and Test 3, respectively. In addition, the center strand (Strand 19) was stressed to $0.50F_u$ during all of the three tests and the remaining wedges were pre-seated to $0.74F_u$. At the end of stressing, the non-center strand was mechanically cut wire-by-wire, followed by the center strand in each test. The strain data were collected at 100 Hz throughout the cutting process.
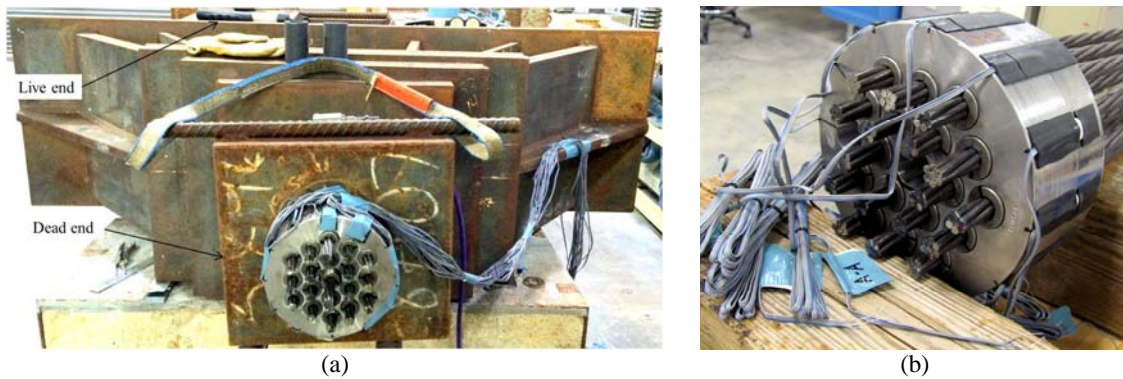

Figure 2.1 Test setup: (a) stressing frame; (b) a close-up of instrumented wedge plate

2.1.2. Experimental results

The wedge plates, especially the portion near the stressed strands, were under significant stress after the stressing step was completed: the strain readings of the nearest gauges in Test 1, Test 2, and Test 3 were -231 $\mu\varepsilon$, -257 $\mu\varepsilon$, and -135 $\mu\varepsilon$, respectively. During the cutting step, well-pronounced strain relief occurred in the wedge plates following each wire cut. For example, after the first wire cut in Strand 1 in Test 1, the compressive strain in Gauge A reduced by approximately 44 $\mu\varepsilon$ (Fig. 2.2a). Fig. 2.2b shows the strain change after equal number of wire cuts on different strand layers. Clearly, wire cuts in an outer layer strand yielded a greater strain relief compared to the inner strands. In addition, the relative strain change among the gauges for a particular strand cut, produced a well-defined peak in Fig. 2.2b, which identified the broken strand. As expected, however, wire cuts in the center strand (Strand 19 located on Layer 4) did not appear to produce a clear peak because all the gauges are equidistant from the corresponding wedge location.
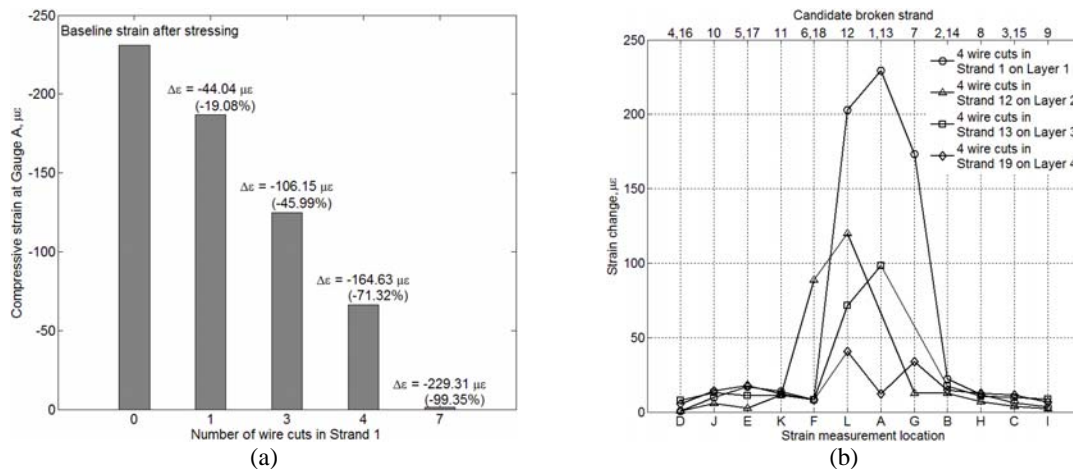

Figure 2.2 Test results: (a) cumulative strain change with wire cuts; (b) wire cuts on different strand layers

2.2. Analytical investigation

An extended study of possible damage scenarios under practical stressing conditions was achieved using an FE model of the PT anchorage assembly. A brief description of the modeling procedure has been provided first, followed by discussions on the analysis results.

2.2.1. FE modeling procedure

To obtain a proper numerical representation of nonlinear, inelastic anchorage behavior, especially contact interactions between different anchorage components (wedges, anchor plate, and bearing plate), a high-resolution FE model is required. Therefore, the 19-strand anchorage volume was discretized with a highly refined mesh: the wedge plate and the bearing plate with approximately 21,000 and 3,000 tri-quadratic (20-node), fully-integrated, hexahedral continuum elements, respectively, and each of the wedges with approximately 1,200 tri-linear (8-node), reduced-integrated hexahedral elements (Fig. 2.3a). An implicit analysis procedure with incrementation-based full Newton iterative method was adopted to obtain the FE solution. In treating the interactions between wedges and wedge plate as well as interaction between wedge plate and bearing plate, penalty-based method was used for enforcing contact constraints and the Coulomb law was used to model the interface friction. A bilinear elasto-plastic material constitutive model was assigned to the wedge plate and bearing plate, whereas a linear-elastic behavior was assumed for the wedges. The displacement degrees of freedom (DOF) of the nodes at the back face of bearing plate was restrained and the anchor was loaded by gradually pressing the wedges into the wedge cavity in the wedge plate. After the wedges were seated into the wedge plate to the target level (for achieving a tendon load of $0.74F_u$), 1/7 of the applied load was removed from a particular wedge to model a wire break.

The magnitude of prestress loss carried to the end anchors, however, is a function of stress recovery away from the break due to interwire friction. A separate numerical study was conducted to investigate the stress recovery, in which a multi-strand tendon was modeled with a stressed strand surrounded by a group of confining strands (Fig. 2.3b). For computational efficiency, the surrounding strands were defined as rigid elements in the finite element analysis (FEA); however, these elements frictionally interacted with the center strand. A wire break was then simulated in the stressed strand by deleting a predefined element set at an intended location of the target wire. An explicit dynamic time integration procedure was used in obtaining the post-breakage response. The analysis results showed significant prestress loss even at distant locations from the break in absence of sufficient external radial pressure. In estimating the amount of applied load to be removed from the target wedge, therefore, a full 1/7 prestress loss for one wire break was assumed (e.g., N/7 of the applied load was removed from a wedge, where N is the number of broken wires) in the previous paragraph. However, a more accurate estimation of load reductions based on stress recovery in deviated tendons is necessary and currently being investigated.

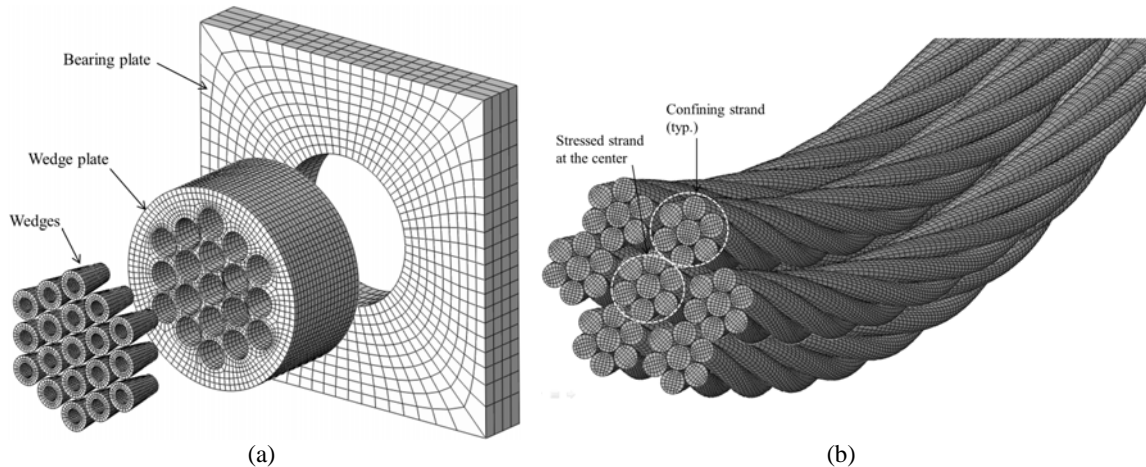(a)   (b)

Figure 2.3 FE model: (a) anchorage; (b) multi-strand tendon

2.2.2. FEA results

The FE model successfully captured the strain change due to simulated wire breaks. Two example wire break scenarios are illustrated in Fig. 2.4a, where one wire break occurred independently in Strand 3 and Strand 7. In each situation, as anticipated, the strain distribution of wedge plate was mostly affected in the region near the

broken strand (Strand 3 and 7). Fig. 2.4b is another representation of strain change around the wedge plate, which more clearly pinpoints the broken strand by showing a peak strain change at the corresponding location on the wedge plate. The relative strain change around wedge plate for various breakage scenarios is shown in Fig. 2.4c. As expected, wire break in an outer layer strand (e.g., Strand 6 on Layer 1) produced a greater strain change compared to inner strands. Moreover, almost equal strain change was observed due to wire breaks in different strands on the same layer (e.g., Strand 8 and 11 both located on Layer 2, as well as Strand 14 and 15 both located on Layer 3). A multiple wire break condition is shown in Fig. 2.4d, where a uniform strain change around the wedge plate was observed due to five (out of seven) wire breaks in Strand 19.
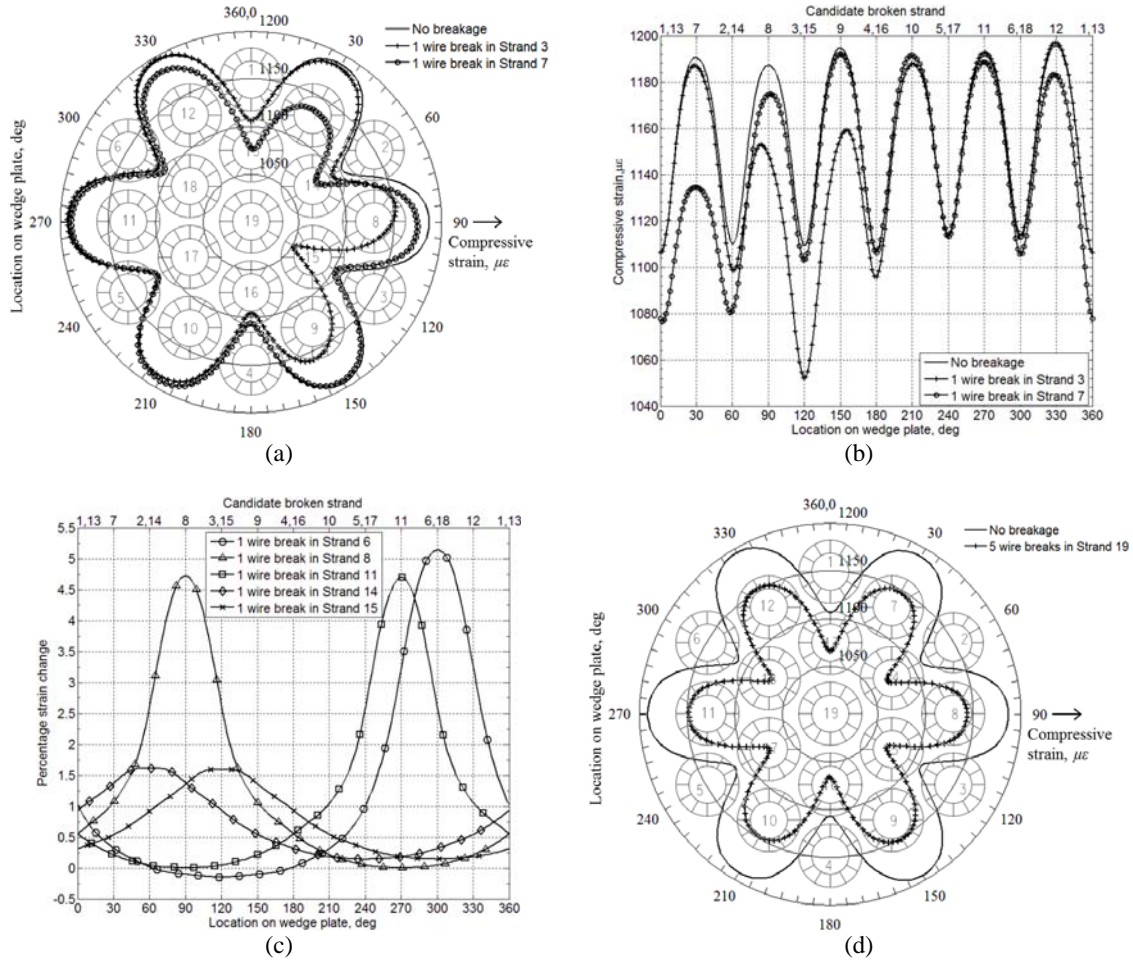

Figure 2.4 Strain change due to wire breaks in strands: (a) 3, 7; (b) 3, 7; (c) 6, 8, 11, 14, 15; (d) 19

2.2.3. Automated damage identification framework

As observed from the experimental and analytical investigations described in the previous sections, the effect of strain relief caused by a wire break in an outer layer strand is limited within a narrow region (not affecting the rest of the wedge plate), which results in a sharp peak in the strain change plot. A breakage in an inner layer strand, on the other hand, distributes the breakage effect on a larger volume of the wedge plate and produces a smaller and distributed peak. Based on these observations, several damage sensitive parameters and their threshold limits were identified for developing a wire breakage detection algorithm. Both absolute strain change at monitoring points and relative strain change among these points, along with their distance from the wedges were taken into account. These parameters were then used in identifying the broken strand layer and finally the damage indices (DIs) were calculated to determine the broken strand (Fig. 2.5). Satisfactory results were obtained when the algorithm was tested for a selected set of threshold values by adding pseudo-random measurement errors (representing imperfect or uneven strain measurement due to defective strain sensors, sensor misalignment, differential temperature at monitoring points, differential wedge seating, and other measurement uncertainties) to the original measured data. A complete and detailed development of this framework can be found in [2, 4].
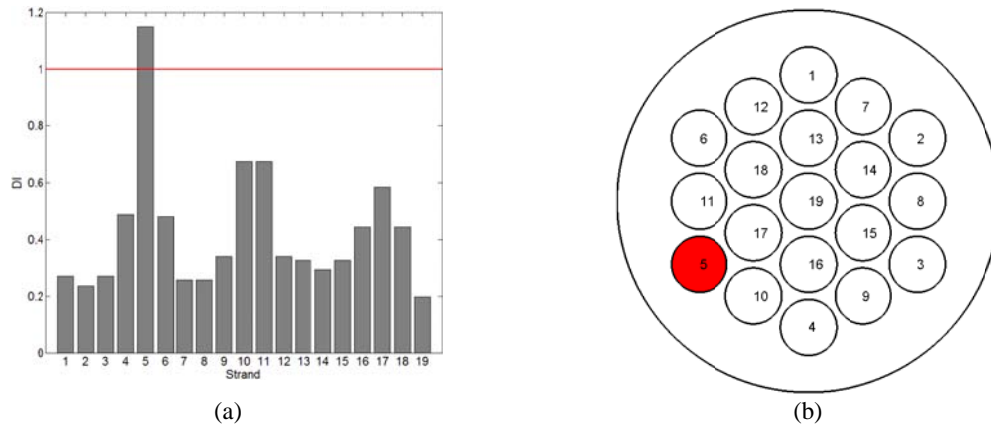
(a)	(b)

Figure 2.5 Automated damage detection: (a) damage indices; (b) visualization of identified tendon damage

3. SENSITIVITY OF STRAND'S NATURAL FREQUENCY TO WIRE BREAKS

A wire break in a prestressing strand modulates its dynamic response through the change in strand's stiffness (due to the loss in cross-sectional area), degree of confinement, and boundary conditions. After the occurrence of a sudden wire break along the strand length, the prestress force at the strand terminations becomes oscillatory, which decays over time until reaching a static equilibrium. Modal properties (e.g., natural frequencies) of the broken strand can be extracted from this oscillatory response time history for detecting wire breakage. This section investigates the change in strand's vibration characteristic, especially the shift of the first longitudinal natural frequency, with successive wire breaks as a criterion for breakage detection.

A laboratory experiment was conducted with a mono-strand tendon for analyzing dynamic post-breakage behavior. The natural frequencies obtained from the experimental measurement gradually decreased with each wire cut. Similarly, an FE model of a strand was prepared for a more detailed investigation on wire breaks. In addition to evaluating strand's post-break dynamic response, the model provided critical information, such as interwire load re-distribution after breakage.

3.1. Experimental investigation

3.1.1. Test setup
An approximately 32-m (105-ft) long prestressing strand was anchored at one end (dead end) with a multi-use chuck and gradually loaded with a mono-strand stressing jack to $0.74F_u$ at the other (live) end. Individual wires were successively cut about 2.5 m (8 ft) away from live end. The strand was passed through a protective hollow steel section to ensure containment of the broken strand after wire cuts (Fig. 3.1). Prestress forces at the ends were continuously recorded by load cells at a high sampling rate (2 kHz) to capture strands' dynamic response.
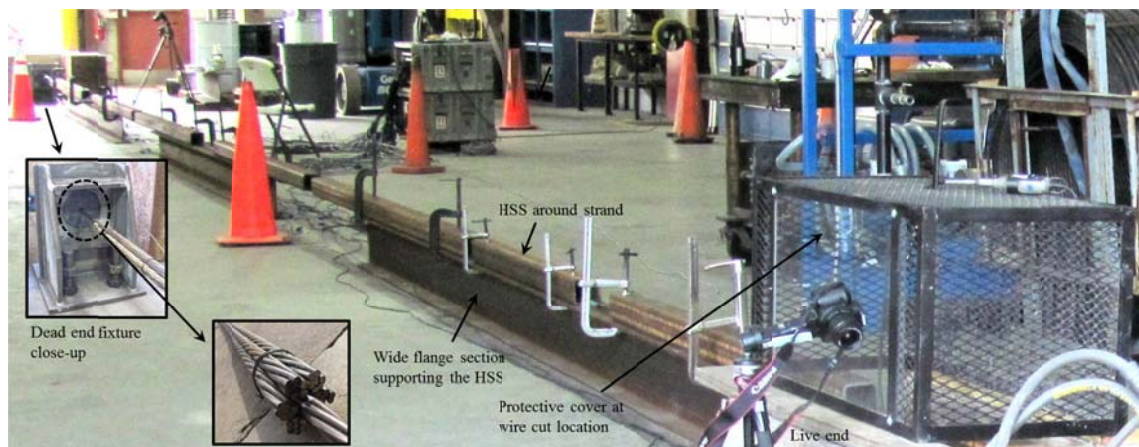

Figure 3.1 Experimental setup

3.1.2. Test results

Fig. 3.2 shows the oscillatory prestress forces recorded by load cell as well as extracted frequencies after the first and third wire cuts. The fundamental longitudinal natural frequency of the strand after the first wire cut (78.08 Hz) decreased from analytically calculated [14] natural frequency of the unbroken strand (80.1 Hz). The frequency continued to decrease with each successive wire cut (e.g., the frequency decreased by almost 10% after the third wire cut), confirming the change in strand's dynamic characteristics.

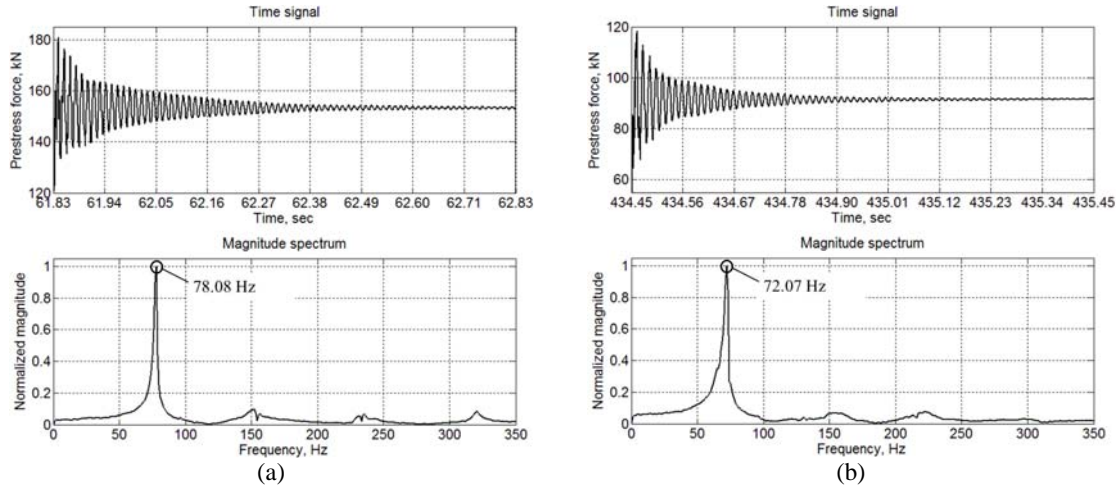(a)   (b)

Figure 3.2 Post-breakage response: (a) after 1 wire break; (b) after 3 wire breaks

3.2. Analytical investigation

3.2.1. FE modeling

The 32-m (105-ft) long strand was modeled using more than one million reduced-integrated, eight-node brick elements. The coefficient of interwire friction was taken as 0.16 [15]. The strand's axial and circumferential DOF at dead end and circumferential DOF at live end was restrained, whereas the axial DOF at live end and radial DOF at both ends were free. Axial prestressing load was gradually applied at the live end through a displacement-controlled loading protocol. Wire breaks were simulated at the same location as in the experimental investigation (approximately 2.5 m away from the live end).

3.2.2. Numerical results

The strand's fundamental longitudinal natural frequency after the first wire break obtained from FEA (77.42 Hz) was in close agreement with the experiment (78.08 Hz). The model also successfully captured the after-breakage load sharing among wires (Table 3.1). At the end nearest to the wire break (live end), the broken wire (Wire 2) lost all its stress and the prestress forces on the adjacent wires (Wire 1, 3, and 5) were increased, whereas forces on the other wires were decreased. These observations are consistent with the literature [15]. The formation of birdcage near live end also indicated the complete loss of prestress on the broken wire (Fig. 3.3). At the dead end (29.5 m away from the break), birdcaging was not observed and the prestress loss was evenly distributed among the wires. However, the total prestress loss at both ends were equal to maintain force equilibrium.

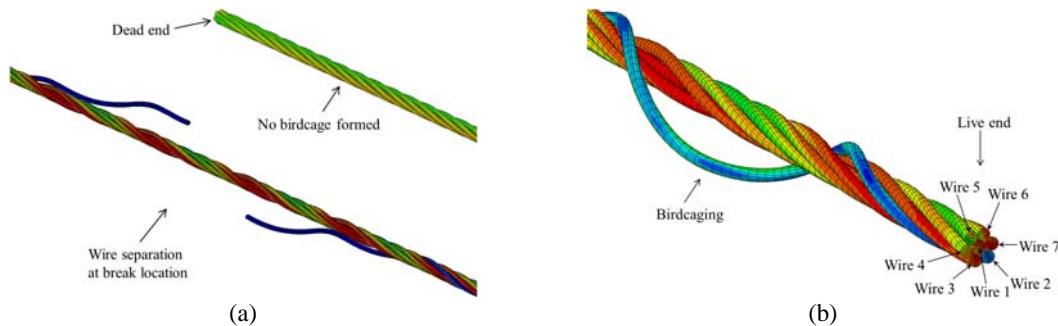(a)   (b)

Figure 3.3 Wire break simulation results: (a) dead end and break location; (b) live end

Table 3.1 Change of prestress force on individual wires after breakage of Wire 2

Wire ID	1	2	3	4	5	6	7
Live end	+25.8%	-99.6%	+13.4%	-5.3%	-20.1%	-1.8%	+12.9%
Dead end	-15.3%	-12.8%	-12.7%	-12.8%	-12.7%	-12.7%	-12.8%

4. CONCLUSIONS

The effectiveness of the two tendon monitoring approaches discussed in this paper have been demonstrated through experimental and analytical investigations. The strain-based approach compares the before- and after-breakage events, and therefore, can be continuous or intermittent, and requires relatively low sampling rate for data acquisition. Nevertheless, feasible options for sensor protection, such as embedding strain sensors into wedge plates during anchor fabrication, is necessary to ensure sensor durability for long-term monitoring. In the frequency-based approach, data must be captured at the time of the breakage event, which requires continuous monitoring with a high sampling rate. Although both the approaches have the advantage of using standard, low-cost sensors and require access only at the end anchors, detecting single wire breaks in inner strands might be challenging under ambient conditions. However, these two approaches can be potentially combined, either using independent sensors or sharing the same sensor array, which would increase their reliability and reduce false positive identification of breakage events.

REFERENCES

1. Corven Engineering. (2002). New Directions for Florida Post-tensioned Bridges. FDOT.
2. Abdullah, A. B. M., Rice, J. A., and Hamilton, H. R. (2015). A Strain-based Wire Breakage Identification Algorithm for Unbonded PT Tendons. *Smart Structures and Systems*. (in press).
3. Abdullah, A. B. M., Rice, J. A., and Hamilton, H. R. (2015). Wire Breakage Detection Using Relative Strain Variation in Unbonded Posttensioning Anchors. *Journal of Bridge Engineering*. **20:1**, 04014056.
4. Abdullah, A. B. M., Rice, J. A., and Hamilton, H. R. (2014). A Damage Detection Model for Unbonded Post-tensioning Tendons Based on Relative Strain Variation in Multi-strand Anchors. *SPIE Smart Structures/NDE*. San Diego, CA.
5. Jimenez, G. A. (2013). Guide for Evaluation and Repair of Unbonded Post-Tensioned Concrete Structures. Post-Tensioning Institute.
6. Salamone, S., Bartoli, I., Phillips, R., Nucera, C., and Lanza di Scalea, F. (2011). Health Monitoring of Prestressing Tendons in Posttensioned Concrete Bridges. *Transportation Research Record*. **2220**, 21–27.
7. Bartoli, I., Salamone, S., Phillips, R., Lanza di Scalea, F., and Sikorsky, C. S. (2011). Use of Interwire Ultrasonic Leakage to Quantify Loss of Prestress in Multiwire Tendons. *Journal of Engineering Mechanics*. **137:5**, 324–333.
8. Della Vedova, M., and Elsener, B. (2006). Enhanced Durability, Quality Control and Monitoring of Electrically Isolated Tendons. *2nd International fib Congress*. Naples, Italy.
9. Iyer, S. R., Sinha, S. K., and Schokker, A. J. (2005). Ultrasonic C-Scan Imaging of Post-Tensioned Concrete Bridge Structures for Detection of Corrosion and Voids. *Computer-Aided Civil and Infrastructure Engineering*. **20:2**, 79-94.
10. Scheel, H., and Hillemeier, B. (2003). Location of Prestressing Steel Fractures in Concrete. *Journal of Materials in Civil Engineering*, **15:3**, 228–234.
11. Matt, P. (2001). Non-destructive Evaluation and Monitoring of Post-tensioning Tendons. *FIB Bulletins*. **15**, 103–108.
12. Ghorbanpoor, A., Borchelt, R., Edwards, M., and Salam, E. A. (2000). Magnetic-based NDE of Prestressed and Post-tensioned Concrete Members. Federal Highway Administration.
13. ASTM. (2006). Standard Specification for Steel Strand, Uncoated Seven-wire for Prestressed Concrete. American Society for Testing and Materials.
14. Meirovitch, L. (1967). Analytical methods in vibrations. The Mcmillan Company.
15. MacDougall, C., and Bartlett, F. M. (2006). Mechanical model for unbonded seven-wire tendon with single broken wire. *Journal of engineering mechanics*. **132:12**, 1345-1353.